Chapter 7

Introduction to interferometry

Contents

Since RSGs are big or relatively nearby, their disk can be resolved with large telescopes using adaptive optics and with the speckle interferometry. This presents a unique way to show how the surface of RSG appears.
In this Chapter I will present some important concepts that will be used in next following. For further details the reader can refer to Shao & Colavita (1992) and Quirrenbach (2001)

7.1 What is Interferometry

The diffraction pattern resulting from a uniformly illuminated circular aperture has a bright region in the center, known as the Airy disc. The following relation shows the angle at which the first minimum occurs

$$\theta = 1.22\frac{\lambda}{\mathrm{D}} \tag{7.1}$$

where θ is the angular resolution in radians, λ is the observing wavelength and D is the diameter of the telescope. This means that with a 10-meter class telescope the resolution

ranges from 20 mas (milli-arcseconds) in the visible (0.8 μm) to 400 mas in the MIR (16 μm). However, the Adaptive Optics is required to correct for the atmospheric turbulence in the visible and NIR.
Optical and Infrared (IR) interferometers are the ideal tools to study the shape and the size of objects which are bright but small and thus they require only a limited light collecting surface, but a high angular resolution and spectral resolution. The science case on very large single dish ($\geq$ 30meters) telescope is under study, but the state of the art is the use of few small telescopes and the combination of the light in such a way as to obtain a high angular resolution (see Fig. 7.1).

Figure 7.1: The Very Large Telescope Interferometer (VLTI) consists in the coherent combination of the four VLT Unit Telescopes (8 meters) and of the four moveable 1.8 meters Auxiliary Telescopes.

The combined light results in the interference pattern: the *fringes*. The van Cittert-Zernike theorem states that the complex quantity (including the phase and the amplitude of the fringes) is the Fourier Transform (FT) of the source intensity distribution on the sky. The original source image can be reconstructed only if one has a good sampling in the uv-plane (the Fourier plane), i.e. if one has a large number of visibility measurements. If one wants to do imaging with interferometric observations, he has to do the inverse FT of a large number of measurements of the fringes contrast and phase. The point is to gain information from different telescope configurations and from a clever way of combining light beams.

7.2 van Cittert-Zernike theorem

It states that the contrast and the phase (location) of the interference pattern (the fringes), i.e. the complex visibility, corresponds to the Fourier Transform of the source intensity distribution on the sky at the spatial frequencies (the conjugates of the two spatial coordinates) corresponding to the baseline projected on the sky.
The complex visibility is a function of the spatial frequencies defined as B/λ (where B is

the baseline, i.e. the distance between two telescopes, and λ is the observing wavelength). These spatial frequency are :

$$\mathrm{u} = \frac{\mathrm{B_x}}{\lambda} \tag{7.2}$$

and

$$\mathrm{v} = \frac{\mathrm{B_y}}{\lambda} \tag{7.3}$$

and they are measured in $arcseconds^{-1}$ or $cycles/arcseconds$.
The normalized visibility can be written as follow

$$\mathrm{V}(\mathrm{u},\mathrm{v}) = \frac{\int \mathrm{d}\alpha\mathrm{d}\beta \mathrm{A}(\alpha,\beta)\,\mathrm{F}(\alpha,\beta)\,\mathrm{e}^{-2\pi\mathrm{i}(\alpha\mathrm{u}+\beta\mathrm{v})}}{\int \mathrm{d}\alpha\mathrm{d}\beta \mathrm{A}(\alpha,\beta)\,\mathrm{F}(\alpha,\beta)} \tag{7.4}$$

where A is the collecting aperture and F the source intensity distribution on the sky, α and β the spatial coordinates. In most cases, one denotes the visibility as the fringes contrast, i.e. $\mid \mathrm{V} \mid$, instead of the complex visibility, and the phase (or fringe location, ϕ) is the arg(V). In other words

$$\mathrm{V} = \mid \mathrm{V} \mid (\cos\phi + \mathrm{i}\sin\phi) \tag{7.5}$$

7.2.1 Properties of Fourier Transform

$$\mathrm{FT}\left[\mathrm{I}_1(\alpha,\beta) + \mathrm{I}_2(\alpha,\beta)\right] = \mathrm{V}_1(\mathrm{u},\mathrm{v}) + \mathrm{V}_2(\mathrm{u},\mathrm{v}) \tag{7.6}$$

$$\mathrm{FT}\left[\mathrm{I}(\mathrm{a}\alpha,\mathrm{b}\beta)\right] = \frac{1}{\mathrm{ab}}\mathrm{V}(\mathrm{u}/\mathrm{a},\mathrm{v}/\mathrm{b}) \tag{7.7}$$

$$\mathrm{FT}\left[\mathrm{I}(\alpha-\alpha_0,\beta-\beta_0)\right] = \mathrm{V}(\mathrm{u},\mathrm{v})\,\mathrm{e}^{2\pi\mathrm{i}(\mathrm{u}\alpha_0+\mathrm{v}\beta_0)} \tag{7.8}$$

$$\mathrm{FT}\left[\mathrm{I}_1(\alpha,\beta) * \mathrm{I}_2(\alpha,\beta)\right] = \mathrm{V}_1(\mathrm{u},\mathrm{v}) \cdot \mathrm{V}_2(\mathrm{u},\mathrm{v}) \tag{7.9}$$

7.3 Basic source morphologies

7.3.1 The point source

The most basic of all intensity profiles is the point source function, i.e. the Dirac function. If the spatial coordinates are (α_0,β_0), the brightness distribution is

$$\mathrm{I}(\alpha,\beta) = \delta(\alpha-\alpha_0,\beta-\beta_0) \tag{7.10}$$

and the visibility is

$$\mathrm{V}(\mathrm{u},\mathrm{v}) = \mathrm{e}^{-2\pi\mathrm{i}(\alpha_0\mathrm{u}+\beta_0\mathrm{v})} \tag{7.11}$$

The amplitude of the visibility is one (the source is not spatially resolved) and the phase is zero if the telescopes are pointed exactly at the source.

7.3.2 Circular symmetric sources : the uniform disk

When the object has a circular symmetry, one can use the distance to the optical axis ($\rho = \sqrt{\alpha^2 + \beta^2}$). In the uv-plane it is

$$\mathrm{r} = \sqrt{\mathrm{u}^2 + \mathrm{v}^2} \tag{7.12}$$

Eq. 7.4 can be simplified as follow (for a transparent derivation see Perrin & Malbet 2003).

$$\mathrm{v}\,(\mathrm{r}) = 2\pi \int_0^\infty \mathrm{I}\,(\rho)\,\mathrm{J}_0\,(2\pi\rho\mathrm{r})\,\rho\mathrm{d}\rho \tag{7.13}$$

which can be normalized with the total flux to find the visibility

$$\mathrm{V}\,(\mathrm{r}) = \frac{\int_0^\infty \mathrm{I}\,(\rho)\,\mathrm{J}_0\,(2\pi\rho\mathrm{r})\,\rho\mathrm{d}\rho}{\int_0^\infty \mathrm{I}\,(\rho)\,\rho\mathrm{d}\rho} \tag{7.14}$$

where r and ρ are defined above, $I\,(\rho)$ is the one-dimensionl intensity profile from the center of the object out to its edge and J_0 is the zeroth-order Bessel function of the first kind. The Eq. 7.13 is the Hankel transform. It is the integral of a whole set of circular, infinitesimally thin rings with a visibility of

$$\mathrm{V}\,(\mathrm{r}) = \mathrm{J}_0\,(2\pi\rho_0\mathrm{r}) \tag{7.15}$$

with a ring radius of ρ_0.
A more useful variable dealing with the intensity profile is:

$$\mu = \sqrt{1 - \left(\frac{\rho}{\rho_{\max}}\right)} \tag{7.16}$$

where $\rho_{\max}$ is the outermost emitting point of the intensity profile. μ is also the cosine of the viewing anlge ($\mu = 1$ is the line-of-sight).
Eq. 7.14 becomes

$$\mathrm{V}\,(\mathrm{r}) = \frac{\int_0^1 \mathrm{J}_0\left(\pi\mathrm{r}\theta\sqrt{1-\mu^2}\right)\mu\mathrm{d}\mu}{\int_0^1 \mathrm{I}\,(\mu)\,\mu\mathrm{d}\mu} \tag{7.17}$$

where θ is the angular diameter of the object.

Within the circular symmetric sources, there is the uniform disk (UD), which correspond to a uniform brightness distribution. Its visibility is

$$\mathrm{V}\,(\mathrm{r}) = 2\frac{\mathrm{J}_1\,(\pi\theta\mathrm{r})}{\pi\theta\mathrm{r}} \tag{7.18}$$

where J_1 is the first-order Bessel function of the first kind (see Fig. 7.14). The UD intensity profile is only the first-order approximation, since one must at least considered a slight decrease of intensity with distance from the center. When the observer is not looking

perpendicularly to the stellar surface, the most of the light comes from more superficial layers as optical depth increase more rapidly with depth than for a perpendicular line-of-sight. As a consequence, we see layer with a lower temperature. The visibility of limb-darkened disk can be compute with Eq. 7.13.
The limb-darkening influences the visibility curve only close to and beyond the first null, and the maximum height of the second lobe of the visibility is a good measure for the amount of limb-darkening. Two examples of analytical approximation of the center-to-limb variation are

$$\mathrm{I}(\mu) = 1 - \mathrm{a}_1 (1 - \mu) \tag{7.19}$$

or

$$\mathrm{I}(\mu) = \nu^{\mathrm{a}_2} \tag{7.20}$$

where I is the intensity, μ is defined in Eq. 7.16, and a_1 together with a_2 are the limb darkening coefficient to be determined with a fit to the observations or to the intensity profiles from radiative transfer code calculations. A large set of synthetic limb darkening coefficients from one-dimensional model atmospheres is in Claret (2000). A reinterpretation of his law adapted to RSG intensity profiles is reported in Sect. 8.3.
Fig. 7.2 reports an example of visibility curve computed from an uniform disk (bottom panel, solid black line) compared to the visibility obtained from the a limb darkened model with a law as in Eq. 7.19 (red dashed curve, a_1=1.5). The two visibilities don't show strong differences in the first lobe. The effect of the center-to-limb variation becomes more evident at the first null point and on height of the second lobe. The limb-darkening effect is small and thus it is necessary an high precision on the visibility measurement.

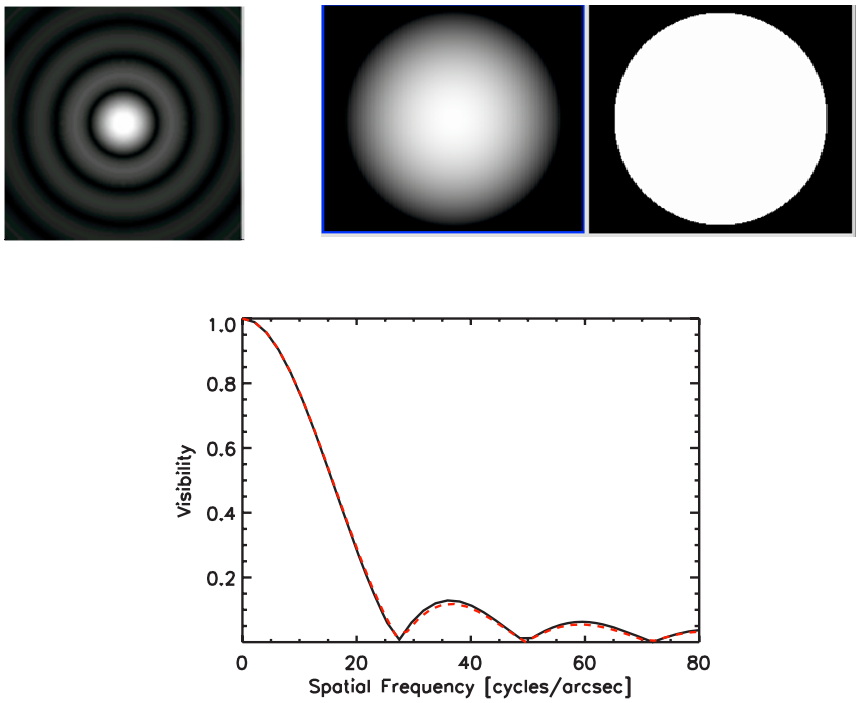

Figure 7.2: *Top left panel:* Fourier transform of a uniform disk model. *Central top panel:* intensity map of a linear center-to-limb variations ($a_1 = 1.5$) with an apparent diameter of 16 mas. *Top right panel:* intensity map of a uniform disk of 16 mas. *Bottom panel:* visibility curves of the uniform disk (black solid line) and of the limb darkened model (red dashed line).

7.4 Closure phase

In Fig. 7.3, an optical interferometer is represented by a Young's two-slit experiment. Flat wavefronts from a distant source impinge on the slits and produce interference pattern on a screen. The spatial frequency of these intensity fringes is determined by the distance between the slits (in units of the wavelength of the illuminating radiation). However, if the pathlength above one slit is changed (due, for example, to a pocket of warm air moving across the aperture), the interference pattern will be shifted by an amount depending on the difference in pathlength ($\Delta\Phi$). If the extra pathlength is half the wavelength, the fringe patter will be shift by half a fringe (π in radians). The phase, i.e. the fringe location, is completely independent of the slit separation and only depends on the slit-specific phase delays.

The loss of this phase information has serious consequences. Imaging can not be done except for simple objects such as disks or "round" stars.
In order to solve this problem, one uses the closure phase for interferometer with more than 2 telescopes. Fig. 7.4 shows that above telescope 2 a phase delay is introduces. This causes a phase shift in the fringe pattern between telescopes 1 and 2. A phase shift is also induced for fringes between telescopes 2 and 3, but this phase shift is equal but opposite to the one for telescopes 1 and 2.

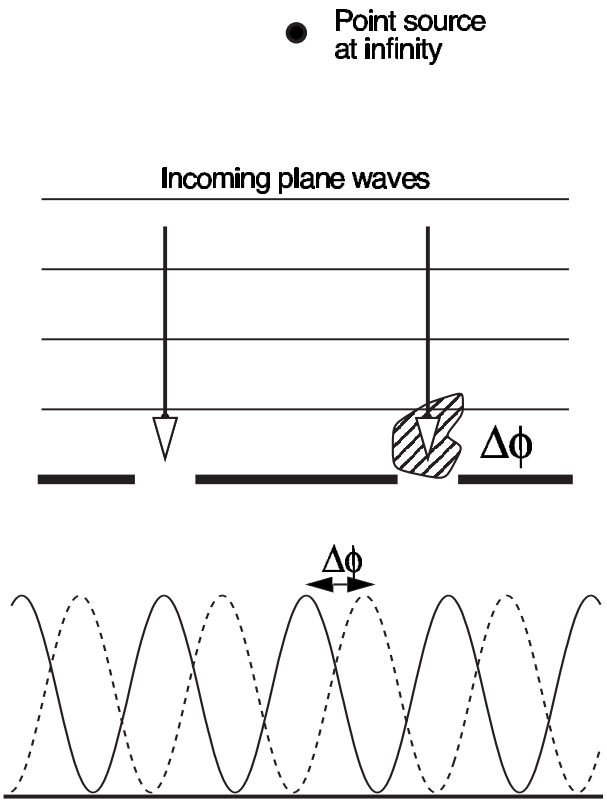

Figure 7.3: Young's two slit experiment used through analogy with optical telescopes to show that phase errors causes fringe shifts.

$$\Phi(1-2) = \Phi_0(1-2) + [\phi(2) - \phi(1)] \tag{7.21}$$

$$\Phi(2-3) = \Phi_0(2-3) + [\phi(3) - \phi(2)] \tag{7.22}$$

$$\Phi(3-1) = \Phi_0(3-1) + [\phi(1) - \phi(3)] \tag{7.23}$$

where Φ is the observed phase, Φ_0 is the intrinsic phase of the object, and ϕ is the phase shift induced by the atmosphere. The sum of the three fringe phases, between $1-2$, $2-3$, and $3-1$ is insensitive to the phase delay above telescope 2. The closure phase (CPh) is:

$$\texttt{CPh}(1-2-3) = \Phi(1-2) + \Phi(2-3) + \Phi(3-1) = \Phi_0(1-2) + \Phi_0(2-3) + \Phi_0(3-1) \tag{7.24}$$

This argument holds for arbitrary phase delays above any of the three telescopes. The interferometric observable, the *closure phase*, is the sum of three phases around a closed triangle of baselines; that is, as mentioned above, independent of telescope-specific phase shifts induced by the atmosphere or optics and gives information on the intrinsic phase of the object. This is indeed very important for complex non-point-symmetric source intensity distribution such as RSG stars are.

Another way to derive the invariance of the closure phase for a specific telescope phase shifts is the *bispectrum*. It is defined as the triple product of the complex visibilities, where ijk correspond to the three telescopes

$$\tilde{B_{ijk}} = \tilde{V_{ij}}\tilde{V_{jk}}\tilde{V_{ki}} \tag{7.25}$$

The bispectrum is a complex quantity and it's phase is identical to the closure phase. The use of the bispectrum for reconstructing diffraction limited images was developed independently of the closure phase by Weigelt (1977) and linked to it later by Roddier (1986). Notice that the bispectrum is always real for source with point symmetry because the closure phases are all 0° or 180° (see Sect. 7.4.2).

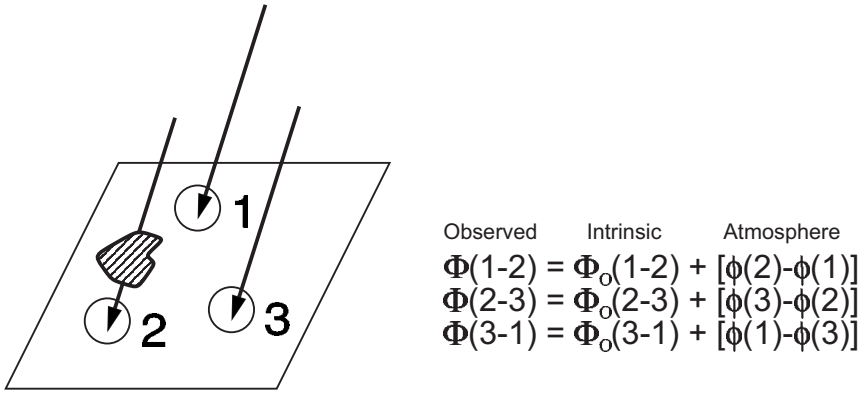

Figure 7.4: The closure phase give phase information important for complex non-point-symmetric source intensity distribution such as RSG stars. At least three or more telescopes are need to correct the atmospheric turbulence.

7.4.1 Important relations

For N telescopes there are

$$\binom{\mathrm{N}}{3} = \frac{(\mathrm{N})\,(\mathrm{N}-1)\,(\mathrm{N}-2)}{(3)\,(2)} \tag{7.26}$$

possible closing triangles. However, there are only

$$\binom{\mathrm{N}}{2} = \frac{(\mathrm{N})\,(\mathrm{N}-1)}{(2)} \tag{7.27}$$

independent Fourier phases because not all the closure phases can be independent. The sum of the independent closure phases is

$$\binom{\mathrm{N}-1}{2} = \frac{(\mathrm{N}-1)\,(\mathrm{N}-2)}{(2)} \tag{7.28}$$

which is equivalent to holding one telescopes fixed and forming all possible triangles with that telescope (Fig. 7.5). The number of independent closure phases is always

less than the number of phases one would like to determine, but the percent of phase information belonging to the closure phases improves as the number of telescopes in the array increases (see Tab. 7.1)

Table 7.1: Phase information recovered by the closure phase

Number of Telescopes	Number of Fourier Phases	Number of Closing Triangles	Number of Independent Closure Phases	Percentage of Phase Information
3	3	1	1	33%
7	21	35	15	71%
21	210	1330	190	90%
27	351	2925	325	93%
50	1225	19600	1176	96%

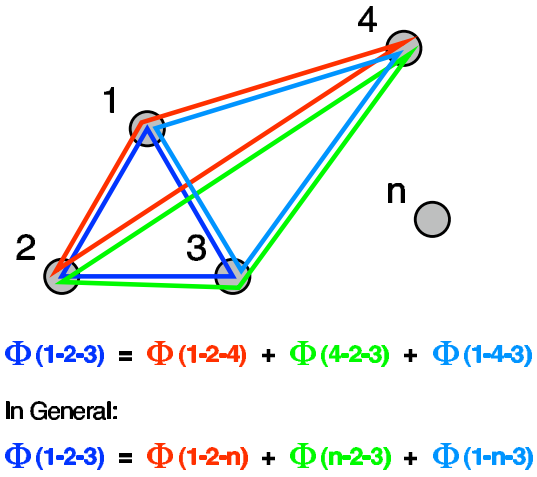

Figure 7.5: The number of combinations for possible closing triangles is not the same as the independent closure phases in the Fourier plan (see text).

7.4.2 Simple cases

The closure phase can vary values from $-180°$ to $180°$ degrees and it is independent of the phase center. In the case of a *binary* or $point-symmetric$ brightness distribution, the closure phase must be either $0°$ or $180°$. In fact, placing the origin (phase center) at the location of point symmetry, the the imaginary part of the Fourier transform disappear (i.e., all odd basis functions must be zero). Hence, the phase of all Fourier components must be either $0°$ or $180°$. In the case of a binary system, one can determine the binary separation (and brightness ratio) from the closure phase information alone, because one would expect to see abrupt closure phase jumps between $0°$ and $180°$ if one of the baselines traverses a null in the visibility pattern (see Fig. 7.6). Notice that the closure phases, or bispectrum, are independent of the telescope-specific phase errors.
The interesting case of a hotspot on stellar surface (see Fig. 7.7) can be thought of as unequal binary with one of the components being resolved. (i) For closing triangles with

all short baselines (compared to the ones needed to spatially resolve the star), the flux from the star itself dominates the visibility measurement and the system looks like centro-symmetric. The resulting closure phase will be small. (ii) for closing triangles containing long baselines, the star is mostly resolved and the hotspot becomes dominant. Also in this limiting case the expected closure phase should be zero. (iii) Only for intermediate baselines, where the star is partially resolved, that non-0° and non-180° values of closure phases are visible. Hence, the fact to have a variety of combinations of closing triangle available is very important to recover the information about the source structure. Without intermediate baselines, one could detect the hotspot, but would only weakly constrain its position on the stellar surface.

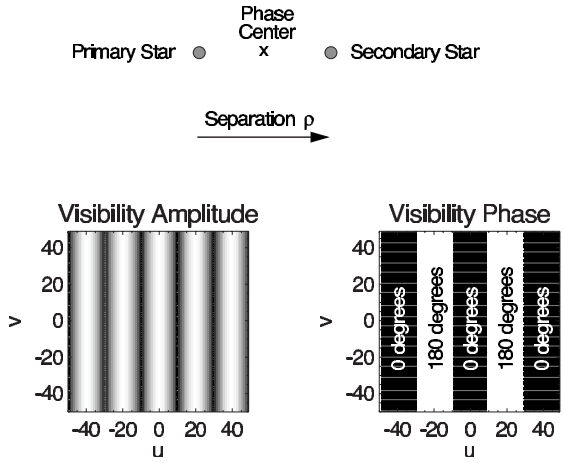

Figure 7.6: The closure phase is independent of the phase center. In the case of a binary system, placing the origin (phase center) at the location of point symmetry, the phase of all Fourier components must be either 0° or 180°. Notice the abrupt phase jumps when visibility goes through a null.

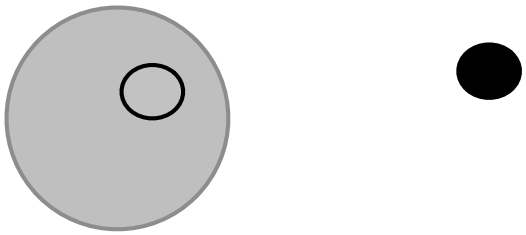

Figure 7.7: Simple model of an hotspot on the stellar surface. *left panel* At low resolution (for closing triangles with all short baselines), stellar disk dominates and it looks like a point symmetric : expected closure phase are small. *right panel* at highest resolution (for closing triangles with all long baselines), stellar disk is spatially resolved and the hotspot by itself is also point symmetric : expected visibilities are close to zero. Only for intermediate baselines, where the star is partially resolved, closure phase have non-0° and non-180° values.

7.5 Interferometer facilities in the world

The list of interferometer facilities in the world is reported in Tab. 7.2. Interferometers give a unique solution for the observation of the surface inhomogeneities of stars like RSG. Today ground interferometers such as, for example, VLTI and CHARA have the possibility to combine the information of the visibility curves together with the closure phases using long baselines together with adaptive optics that increase the sensitivity and angular resolution. This is of extreme importance for the reconstruction of the observed stars.
In the near-future, a large and more complete coverage of the uv-plane will finally probe an intensity map really close the observed one. This will be of extreme interest to constrain the simulations such as CO^{5}BOLD, that can provide detailed intensity maps.

Table 7.2: Interferometer facilities in the world

Facility Acronym	Operating Institution	Location	No. of Aper.	Size of Aper.[cm]	Maximum Baseline [m]	Wavelength Range	Starting operating
GI2T	Obs. Côte d'Azur	Calern France	2	150	70	Vis.	1985 to 2005
ISI	UC Berkeley	Mt. Wilson USA	3	165	30+	MIR	1990
COAST	Cambridge University	Cambridge United Kindom	5	40	22	Vis. & NIR	1991
SUSI	Sydney University	Narrabri Australia	13	14	640	Vis.	1991
IOTA[a]	CfA/U Mass	Mt. Hopkins USA	3	45	38	Vis. & NIR	1993 to 2006
NPOI	USNO/NRL	Anderson Mesa USA	6	60	435	Vis.	1995
PTI	JPL/Caltech	Mt. Palomar USA	2	40	110	NIR	1995
MIRA-I	NAO Japan	Tokyo Japan	2	25	4	Vis.	1998
CHARA	Georgia St. University	Mt. Wilson USA	6	100	350	Vis. & NIR	1999
KI	CARA	Mauna Kea USA	2	1000	85	NIR & MIR	2001
VLTI [b]	ESO	Cerro Paranal Chile	4(8)	820 (180)	200	NIR & MIR	2002

[a]Interferometric data from this telescope will be used for the comparison with RHD simulations
[b]I detail the prospects for the detection and characterisation of granulation (contrast, size) on RSG with this interferometer